

Turbulence and passive scalar transport in a free-slip surface

Bruno Eckhardt and Jörg Schumacher*

Fachbereich Physik, Philipps-Universität Marburg, D-35032 Marburg, Germany

(Received 6 December 2000; published 25 June 2001)

We consider the two-dimensional (2D) flow in a flat free-slip surface that bounds a three-dimensional (3D) volume in which the flow is turbulent. The equations of motion for the two-dimensional flow in the surface are neither compressible nor incompressible but strongly influenced by the 3D flow underneath the surface. The velocity correlation functions in the 2D surface and in the 3D volume scale with the same exponents. In the viscous subrange the amplitudes are the same, but in the inertial subrange the 2D one is reduced to 2/3 of the 3D amplitude. The surface flow is more strongly intermittent than the 3D volume flow. Geometric scaling theory is used to derive a relation between the scaling of the velocity field and the density fluctuations of a passive scalar advected on the surface.

DOI: 10.1103/PhysRevE.64.016314

PACS number(s): 47.27.Gs, 47.53.+n, 92.10.Lq

I. INTRODUCTION

We consider flows in a flat two-dimensional (2D) surface that bounds a three-dimensional (3D) volume with turbulent fluid motion. The boundary condition is that of a free-slip surface so that the normal velocity component vanishes but the parallel components are not further constrained. To some extent, this is the situation of surface currents on a river or the sea, if waves and ripples are absent or can be neglected. Particles floating on the surface reflect the properties of the flow and provide an easy visualization. These flows have an obvious connection to oceanographic applications [1,2], but they apparently have not been studied in further detail. Even in the recent theoretical and experimental investigations of the statistical properties of the particle distribution by Ott and co-workers [3–6] the modeling was based on random dissipative maps and not on the underlying flow. Similarly, Saichev and co-workers [7,8] based their investigation of passive particle advection and cluster formation on Gaussian random velocity fields, white in time. Thus, one of our aims here is to analyze the properties of surface flows arising from Navier-Stokes dynamics and to connect them to the statistics of particles floating on the surface, along the lines of our previous work on passive scalars advected in two-dimensional turbulent flows [9].

The flow in the surface is two dimensional, but it has properties that are different from those of the usual two-dimensional incompressible Navier-Stokes turbulence. Obviously, the velocity field is not constrained by mass conservation in the surface: there can be up- and downwelling motions in the (incompressible) bulk which on the surface will appear as sources and sinks for the velocity field. Velocity and vorticity can be exchanged with the bulk flow underneath, so that in the inviscid limit without forcing neither kinetic energy nor enstrophy are conserved. Such effects of compressibility arise also in experiments in two-dimensional turbulence in soap films and were discussed recently [10–12].

The experiments of Goldberg *et al.* [13] are close to a laboratory realization of the kinds of flow that are investigated here. A vertically oscillating grid in a tank of water is used to produce turbulence. If the water surface is sufficiently far away from the grid it remains essentially flat and the surface flow can be visualized with mushroom spores. The measured statistical properties of the flow are close to the ones that we will derive here. This opens the way to further experimental studies of the statistical properties of the velocity field and of the particle dynamics in this interesting flow.

Finally, we should like to point out that the flows are also of interest from a theoretical point of view, since they can be thought of as flows with a symmetry plane. Let the surface be $z=0$ and consider the reflection symmetry that as $z \rightarrow -z$ the z component of the velocity field changes sign. This is a symmetry of the Navier-Stokes equation, that is to say, if initial conditions and driving preserve this symmetry so does the time evolved flow.

It is our aim here to derive the equations of motion for such a flow (Sec. II A), to discuss the correlation function if the 3D flow is turbulent (Sec. II B), to present numerical results on the statistics of the velocity, vorticity, and divergence fields and on the boundary layer thickness (Sec. III), and to derive a relation between the fractal dimension and the velocity correlation function for the advection of scalars within geometric scaling theory (Sec. IV). Concluding remarks are given in Sec. V.

II. THE TWO-DIMENSIONAL FLOW IN A FREE-SLIP SURFACE

In order to arrive at the properties of such a flow, two approaches are possible: one relies on an explicit representation of the flow field with proper boundary conditions and the other seeks to derive the equations of motion from the 3D Navier-Stokes equation. They provide complementary information on the system.

A. Flow with reflectional symmetry

We begin with the equations of motion and the effects of symmetry. Let u , v , and w be the x , y , and z components of

*Present address: P.O. Box 208284, Yale University, New Haven, CT 06520-8284.

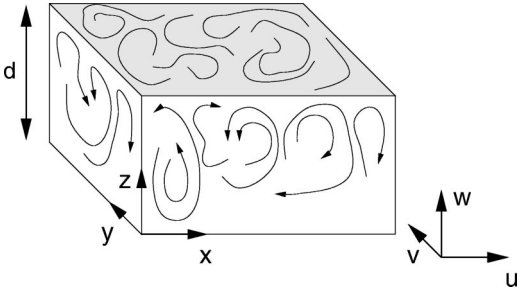


FIG. 1. Flow geometry. The surface flow exists in the shaded surface above a turbulent bulk flow. x and y are the coordinates in the surface and z is the one normal to it. In the numerical simulation the flow is driven by a shear flow in the x direction with variations in z .

the velocity field (Fig. 1) and let p be the pressure field. The surface flow can be realized as flow in a symmetry plane, e.g., the plane $z=0$ if the velocity field is invariant under the symmetry $(u, v, w) \rightarrow (u, v, -w)$ when $z \rightarrow -z$. This suggests expanding the velocity components in power series in z , with only odd powers for w , and only even ones for u , v , and p ,

$$u(x, y, z, t) = \sum_{n=0}^{\infty} u_{2n}(x, y, t) z^{2n}, \quad (1)$$

$$v(x, y, z, t) = \sum_{n=0}^{\infty} v_{2n}(x, y, t) z^{2n}, \quad (2)$$

$$w(x, y, z, t) = \sum_{n=0}^{\infty} w_{2n+1}(x, y, t) z^{2n+1}, \quad (3)$$

and

$$p(x, y, z, t) = \sum_{n=0}^{\infty} p_{2n}(x, y, t) z^{2n}. \quad (4)$$

Substitution into the Navier-Stokes equation and ordering with respect to powers of z gives for the two main components of interest, $u_0(x, y, t)$ and $v_0(x, y, t)$, the equations

$$\partial_t u_0 + (\hat{\mathbf{u}}_0 \cdot \hat{\nabla}) u_0 = -\partial_x p_0 + \nu \hat{\Delta} u_0 + 2\nu u_2 + f_u, \quad (5)$$

$$\partial_t v_0 + (\hat{\mathbf{u}}_0 \cdot \hat{\nabla}) v_0 = -\partial_y p_0 + \nu \hat{\Delta} v_0 + 2\nu v_2 + f_v. \quad (6)$$

The carets on position vectors \mathbf{x} and \mathbf{R} , on the velocity field \mathbf{u} , on the gradient ∇ , and on the Laplace operator Δ indicate that they are restricted to the components x and y that lie in the surface. The driving of the turbulence is modeled by a volume force with components f_u , f_v , and f_w ; as usual we expect that the statistical properties of the flow will depend only weakly (through intermittency) on the kind of driving as long as it is confined to large scales. ν is the kinematic viscosity of the fluid.

For the full 3D velocity field mass conservation $\nabla \cdot \mathbf{u} = 0$ connects the normal and tangential components, viz., $\partial_z w = -\partial_x u - \partial_y v$ or, on the levels of the components [cf. Eqs. (1)–(3)],

$$w_{2n+1} = -(\partial_x u_{2n} + \partial_y v_{2n}) / (2n+1). \quad (7)$$

Similarly, the pressure has to be determined from the 3D relation $\Delta p = -\nabla \cdot [(\mathbf{u} \cdot \nabla) \mathbf{u}]$. With the power series expansion from above this becomes to leading order in z

$$\hat{\Delta} p_0(x, y) + 2p_2(x, y) = 2[(\partial_x u_0)(\partial_y v_0) - (\partial_y u_0)(\partial_x v_0)] - 2(\partial_x u_0 + \partial_y v_0)^2. \quad (8)$$

Equations (5), (6), and (8) are the equations of motion for the surface flow. Note that besides the surface velocity field (u_0, v_0) and the surface pressure p_0 there are additional contributions from higher order terms in the power series in z : the viscous driving terms νu_2 and νv_2 from shear effects in the normal direction and a contribution $(\hat{\Delta})^{-1} p_2$ to the pressure, also resulting from pressure variations in the wall normal direction. From the point of view of the flow in the surface, these terms are externally given and can hence be included in the volume driving forces. Note, however, that now the driving is no longer confined to large scales, as assumed in the usual scaling analysis. With all unspecified terms absorbed into effective volume forces \tilde{f}_u and \tilde{f}_v , the equations of motion for u_0 and v_0 become finally

$$\partial_t u_0 + (\hat{\mathbf{u}}_0 \cdot \hat{\nabla}) u_0 = -\partial_x p_0 + \nu \hat{\Delta} u_0 + \tilde{f}_u, \quad (9)$$

$$\partial_t v_0 + (\hat{\mathbf{u}}_0 \cdot \hat{\nabla}) v_0 = -\partial_y p_0 + \nu \hat{\Delta} v_0 + \tilde{f}_v, \quad (10)$$

The equations are completed by Eq. (8) with $p_2=0$ for the pressure.

These equations have unusual properties. For instance, dotting with $\hat{\mathbf{u}}$ and integrating over a 2D volume, the energy is not conserved in the Eulerian limit where viscosity and driving are absent. With the local energy density

$$E(x, y, t) = (u_0^2 + v_0^2) / 2, \quad (11)$$

and using Eq. (7) for $n=0$ the global energy balance reads

$$\partial_t \langle E(x, y, t) \rangle_S = -\langle w_1(x, y, t) [E(x, y, t) + p_0(x, y, t)] \rangle_S, \quad (12)$$

where $\langle \cdot \rangle_S$ denotes the average over the surface S . Thus energy is permanently put in and taken out according to the gradients of the z component of \mathbf{u} and the pressure fluctuations. Over large time intervals one can expect that a flow equilibrium with constant average energy is established and that the time average of the right hand side of Eq. (12) vanishes. It seems that the lack of energy conservation for short times gives rise to larger fluctuations and larger intermittency corrections (see below and [13]). A similar discussion applies to the vorticity, and will be given in Sec. III B below.

B. Direct representation of a stress-free surface

The alternative approach mentioned above starts from an explicit representation of the 3D velocity field that takes the boundary conditions into account. Consider the Fourier expansion of the velocity field,

$$u(x, y, z, t) = \sum_{\hat{\mathbf{K}}, n} u_{\hat{\mathbf{K}}, n}(t) \exp(i\hat{\mathbf{K}} \cdot \hat{\mathbf{x}}) \cos(n\pi z), \quad (13)$$

$$v(x, y, z, t) = \sum_{\hat{\mathbf{K}}, n} v_{\hat{\mathbf{K}}, n}(t) \exp(i\hat{\mathbf{K}} \cdot \hat{\mathbf{x}}) \cos(n\pi z), \quad (14)$$

$$w(x, y, z, t) = \sum_{\hat{\mathbf{K}}, n} w_{\hat{\mathbf{K}}, n}(t) \exp(i\hat{\mathbf{K}} \cdot \hat{\mathbf{x}}) \sin(n\pi z), \quad (15)$$

where the summation extends over all 2D wave vectors $\hat{\mathbf{K}} = (K_x, K_y)$ in the surface and all integers n . The sine and cosine terms take into account the stress-free boundary conditions at the top and bottom surfaces,

$$\partial_z u = \partial_z v = w = 0 \quad \text{for } z=0 \quad \text{and } z=1. \quad (16)$$

Incompressibility requires that

$$iK_x u_{\hat{\mathbf{K}}, n} + iK_y v_{\hat{\mathbf{K}}, n} + n\pi w_{\hat{\mathbf{K}}, n} = 0. \quad (17)$$

One advantage of this representation is that it quickly leads to a prediction for the two-point correlation functions. In the 3D case Kolmogorov scaling without intermittency gives for the inertial regime a decay of amplitudes $|\mathbf{u}_{\hat{\mathbf{K}}, n}|^2 \propto |\hat{K}^2 + (n\pi)^2|^{-11/3}$ [14]. In the surface, the 2D amplitudes are obtained by summation on n . This brings in a factor of K that compensates the one missing from the volume element, which is $K dK$ in 2D rather than $k^2 dk$ as in 3D. As a net result scaling of the correlation function does not change. However, the absence of the third component of the velocity field reduces the amplitude to two-thirds of its three-dimensional value. For the second order structure function, defined as

$$S_2(R) = \langle |\mathbf{u}(\mathbf{x} + \mathbf{R}) - \mathbf{u}(\mathbf{x})|^2 \rangle, \quad (18)$$

we expect in the inertial regime

$$\hat{S}_2(R) = \frac{2}{3} S_2(R) \sim R^{2/3}, \quad (19)$$

where again the caret distinguishes the 2D surface from the 3D bulk structure function.

III. NUMERICAL SIMULATIONS

The numerical simulations are based on a nearly homogeneous turbulent shear flow bounded by stress-free surfaces at $z=0$ and $z=1$ as given in Eq. (16). The velocity field is decomposed as in Eqs. (13)–(15) and the Navier-Stokes equations are integrated using a pseudospectral method [15,16]. The simulations were done for Taylor Reynolds numbers $\text{Re}_\lambda = 59, 79$, and 99 , calculated from the streamwise velocity component u , i.e., $\text{Re}_\lambda = u_{rms}^2 / [(\partial_x u)^2]^{1/2} \nu$ with root mean square velocity $u_{rms} = \langle u^2 \rangle^{1/2}$. The properties of the 3D bulk flow are included here only to the extent that they are needed for the comparison between bulk and surface; they are further analyzed in [16].

Kolmogorov length $\eta = (\nu^3/\epsilon)^{1/4}$, velocity $v_\eta = (\epsilon\nu)^{1/4}$,

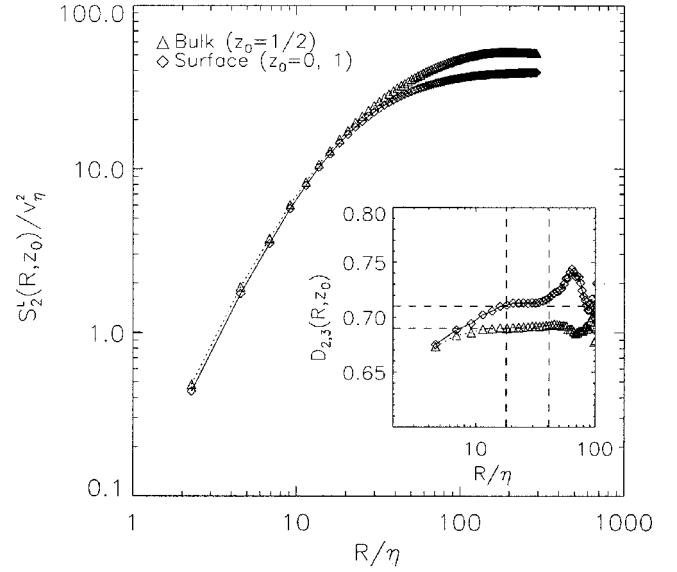


FIG. 2. Second order structure functions $\hat{S}_2^L(\hat{R}, z_0)/v_\eta^2$ for $\text{Re}_\lambda = 99$ normalized with $v_\eta = (\epsilon\nu)^{1/4}$ and ϵ from Eq. (20). Data from the surfaces at $z_0=0$ and $z_0=1$ are indicated by diamonds and connected by continuous lines. Data in the bulk were taken at $z_0=1/2$ and are indicated by triangles and dashed lines. The inset shows the local scaling exponents from an extended self-similarity (ESS) analysis. Estimates between the vertical dashed lines, where the exponents are reasonably constant, give mean scaling exponents of 0.69 in the bulk and 0.71 in the surface. These values are indicated by horizontal dashed lines.

and time scales $\tau_\eta = (\nu/\epsilon)^{1/2}$ are calculated from the 3D energy dissipation rate in the surface, i.e.,

$$\epsilon = \nu \sum_{i,j=1}^2 \langle (\partial_i u_j)^2 \rangle_S + \nu \langle (\partial_3 u_3)^2 \rangle_S, \quad (20)$$

where indices 1, 2, and 3 correspond to x , y , and z , respectively. For $\text{Re}_\lambda = 99$ this dissipation rate in the surface is about 40% of the value in the bulk.

A. Structure functions of the velocity field

Form factors in the middle of the cell and on the surface are determined from 114 statistically independent snapshots of the turbulent flow. We focus on the scaling of the n th order longitudinal structure functions, defined as

$$\hat{S}_n^L(\hat{R}, z_0) = \langle |[\hat{\mathbf{u}}(\hat{\mathbf{x}} + \hat{\mathbf{R}}, z_0) - \hat{\mathbf{u}}(\hat{\mathbf{x}}, z_0)] \cdot \hat{\mathbf{R}}/\hat{R}|^n \rangle. \quad (21)$$

In the bulk and without intermittency corrections the second order structure function is expected to scale like R^2 in the viscous subrange and like $R^{2/3}$ in the inertial subrange [14]. A comparison between bulk and surface structure functions is shown in Fig. 2 for $\text{Re}_\lambda = 99$. The two structure functions coincide in the viscous subrange but differ in the inertial subrange. This difference is predominantly in the amplitude and not in the scaling exponents, and is consistent with Eq. (19). A local scaling exponent can be defined as $\zeta(\hat{R}) = d \ln \hat{S}_n^L(\hat{R}, z_0) / d \ln \hat{R}$. Unfortunately, the two structure func-

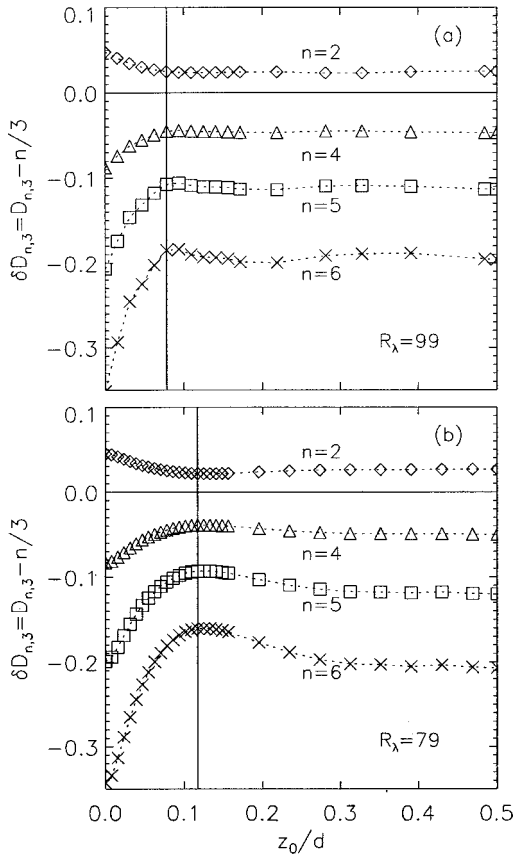


FIG. 3. Deviations of the local ESS scaling exponent from the classical Kolmogorov scaling for different heights z_0 of the averaging plane and for different orders $n=2$ to $n=6$. Part (a) for $Re_\lambda = 99$, averaged over 228 samples. The deviations $D_{n,3}(R, z_0)$ are the mean obtained for scales R between 18η and 41η , as indicated by vertical lines in the inset of Fig. 2. Part (b) for $Re_\lambda = 79$, averaged over 254 samples. Here the exponents are obtained for scales R between 10η and 27η . The vertical lines indicate the surface layer that is analyzed further in Sec. III D.

tions do not show an algebraic scaling behavior at intermediate scales between the viscous and the forcing scale range for the values of Re_λ achieved here. Therefore, we apply the extended self-similarity (ESS) analysis [17] to the data. A local ESS scaling exponent can be calculated by relating local scaling exponents of second and third order structure functions,

$$D_{2,3}(\hat{R}, z_0) = \frac{d \ln[\hat{S}_2^L(\hat{R}, z_0)]}{d \ln[\hat{S}_3^L(\hat{R}, z_0)]}. \quad (22)$$

The distance vector \hat{R} is taken in planes of fixed z_0 . As shown in the inset in Fig. 2 the bulk data give a local scaling exponent of about 0.69, in agreement with other observations, but in the surface the local slope is larger, about 0.71. This difference is small but statistically significant. Local exponents, based on averages over planes parallel to the surface, show almost no variation in the center of the cell but a clear trend when approaching the surface. This is demonstrated in Fig. 3 for the deviations $\delta D_{n,3}(R, z_0)$

$= D_{n,3}(R, z_0) - n/3$ from classical Kolmogorov scaling [14] for orders $n=2$ to $n=6$ for different z_0 . The plane $z_0 = 1/2$ defines the middle between both free surfaces. Data sets for two different Taylor-Reynolds numbers $Re_\lambda = 99$ (a) and 79 (b) are shown. The transition from bulk to surface behavior can be used to define a surface layer, as discussed further in Sec. III D.

The increase in intermittency seems to be connected with an increase in fluctuations due to lack of incompressibility and lack of energy conservation. It is in line with results for passive scalar transport in models with compressible Gaussian random flows that are δ correlated in time [18,19] and with direct numerical simulations [20,21] of isotropic supersonic turbulence. Interestingly, in the latter case the authors also noted a strong difference from incompressible turbulence near the crossover to the viscous subrange. In their case vortex filaments of high intensity and narrow regions of strong negative divergence, due to small scale supersonic shocks, appeared. In our situation it is the fluctuations due to normal shear and normal velocity components below the surface that have a strong effect near the crossover to the viscous subrange.

In the viscous subrange the amplitudes of the structure functions agree, but in the inertial subrange the surface structure function is smaller by a factor of $2/3$. In the previous section we explained the reduction in amplitude in the inertial range by the reduction in the number of active degrees of freedom or Fourier modes. In the viscous subrange this argument does not apply, since we absorbed many additional contributions to the equations of motion into the volume driving force. The amplitude is larger since these extra contributions also have to be dissipated, but it should not exceed that of a 3D structure function since they originally come from a 3D flow. So in the viscous subrange the reduction in dimensionality is not noticeable and the structure functions coincide.

B. Structure function of the vorticity field

Another quantity of interest in 2D flows is the vorticity $\omega = \partial_x v - \partial_y u$ and its structure function

$$\hat{\Omega}(\hat{R}) = \langle |\omega(\hat{\mathbf{x}} + \hat{\mathbf{R}}) - \omega(\hat{\mathbf{x}})|^2 \rangle. \quad (23)$$

In 2D incompressible turbulence squared vorticity is an additional inviscid invariant and gives rise to an inverse cascade of energy. In 3D a vortex stretching term $(\boldsymbol{\omega} \cdot \nabla) \mathbf{u}$ is present that prevents a conservation of enstrophy. In 2D and for the normal component of the vorticity this reduces to a normal gradient of the velocity field which by incompressibility is connected to the divergence of the flow field in the surface. Thus, for the 2D free surface flow the vorticity transport equation reads

$$\partial_t \omega + (\hat{\mathbf{u}} \cdot \hat{\nabla}) \omega = -\omega(\hat{\nabla} \cdot \hat{\mathbf{u}}) + \nu \hat{\Delta} \omega + \tilde{f}_\omega, \quad (24)$$

and the nonvanishing divergence of the surface flow provides a kind of additional vorticity forcing in 2D. Consequently, squared vorticity cannot be an inviscid invariant, and no inverse cascade develops.

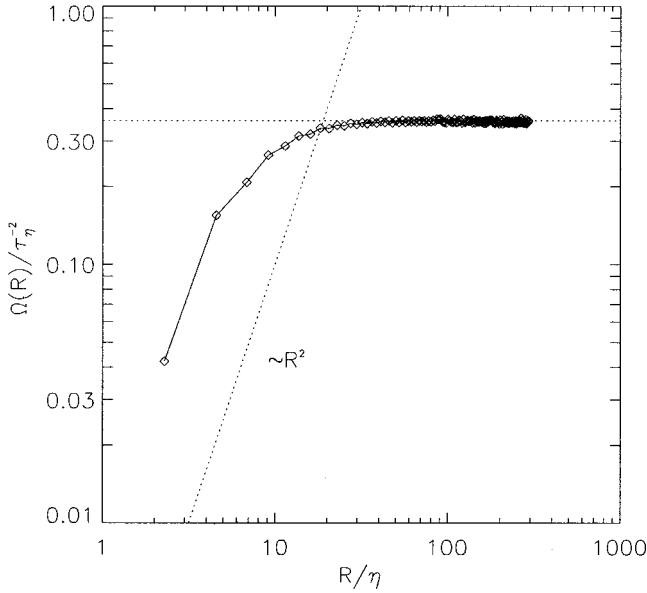


FIG. 4. Vorticity structure function $\Omega(R)/\tau_\eta^{-2}$ for the surface flow at $Re_\lambda = 99$. The data base is the same as for Fig. 2.

The vorticity structure function for the data underlying Fig. 2 is shown in Fig. 4. It saturates for larger separations to a nonvanishing value. Nonvanishing vorticity fluctuations were also observed in experiment [13] and interpreted as an indication that the observed features are not connected with turbulent surface waves [22]. Note that in incompressible stationary turbulence the second order velocity and the second order vorticity structure function are connected by an exact relation $\Omega(R) = 2\epsilon/\nu - \Delta S_2(R)$ [23,24]. This holds true in two and three dimensions, but has additional terms if the flows are not incompressible.

The strong intermittency of the flow is also reflected in the probability density function. Figure 5 shows that the probability density function of the vorticity deviates from a Gaussian distribution and has the exponentially stretched tails that are typical for intermittent quantities.

C. Divergence of the surface flow

The property that distinguishes surface flows from incompressible 2D flows most clearly is the divergence of the flow, which does not vanish for the surface flow. Snapshots of the flow field, such as in Fig. 6, clearly show the presence of sources and sinks. A vertical slice across the flow underneath the surface allows one to connect them to up- and downwelling motions below the surface. The corresponding contour plot of the divergence of the surface flow (Fig. 7) shows randomly fluctuating patches of sources and sinks. In the mean the flow is divergence free, $\langle (\hat{\nabla} \cdot \hat{\mathbf{u}}) \rangle = 0$, but the root mean square value does not vanish. Formally one can define a compressibility factor [18]

$$0 \leq C = \frac{\langle (\hat{\nabla} \cdot \hat{\mathbf{u}})^2 \rangle}{\langle |\hat{\nabla} \hat{\mathbf{u}}|^2 \rangle} \leq 1, \quad (25)$$

which relates the mean square divergence to the mean square

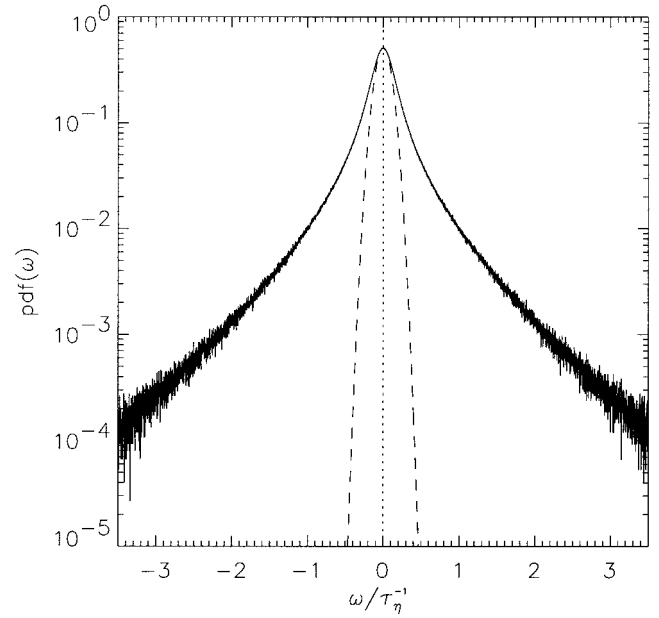


FIG. 5. Probability density function (PDF) of the surface vorticity component for the flow field of Fig. 2. For comparison a Gaussian PDF fitted to the central part of the distribution is indicated as well (dashed line).

velocity gradient. For the surface flow and using only the velocity components in the surface, this becomes

$$C = \frac{\langle (\hat{\nabla} \cdot \hat{\mathbf{u}})^2 \rangle}{\langle |\hat{\nabla} \hat{\mathbf{u}}|^2 \rangle}. \quad (26)$$

In our simulations for $Re_\lambda = 99$ we find $C \approx 1/2$, in good agreement with the experiments of Goldburg *et al.* [13]. The relation of the denominator in Eq. (26) to the energy dissipation rate (20) is given by

$$\epsilon = \nu [\langle |\hat{\nabla} \hat{\mathbf{u}}|^2 \rangle_S + \langle (\hat{\nabla} \cdot \hat{\mathbf{u}})^2 \rangle_S] = \nu \langle |\hat{\nabla} \hat{\mathbf{u}}|^2 \rangle_S (1 + C). \quad (27)$$

The mean extension of regions with similar divergence can be determined from the correlation function

$$C_{div}(\hat{R}) = \langle [(\hat{\nabla} \cdot \hat{\mathbf{u}}(\hat{\mathbf{x}}))][(\hat{\nabla} \cdot \hat{\mathbf{u}}(\hat{\mathbf{x}} + \hat{R}))] \rangle. \quad (28)$$

This correlation function is shown in Fig. 8. The first zero of $C_{div}(\hat{R})$ defines a decorrelation length scale L_{div} ; in units of the Kolmogorov scale $L_{div} \approx 25$. This scale fits rather well with the size of the largest patches in Fig. 7. As a consequence, the term in Eq. (24) that contains the divergence of the velocity field describes a driving force that can be expected to be confined to the smaller scales in the flow.

D. Fluctuations of the vertical velocity component

In Sec. III A we already mentioned the variations of the statistical properties with distance from the surface. They allow us to identify a surface layer in which the transition from bulk to surface behavior takes place. This layer is different from the ones near rigid walls and is not connected to

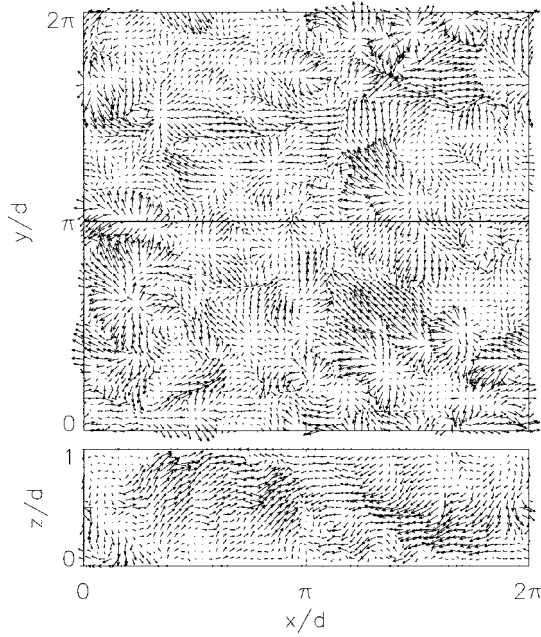


FIG. 6. A turbulent velocity field in the free-slip surface flow for $Re_\lambda = 99$. The upper panel shows a vector plot of the components u and v in the surface at $z/d = 0$. The lower panel shows a vertical cut through the box at the horizontal line ($y/d = \pi$) marked in the upper panel. Regions of rising fluid and sinking fluid in the lower panel can be connected to sources and sinks near the solid line in the upper panel.

friction but rather to the suppression of velocity fluctuations in the wall-normal direction. Dimensional arguments allow us to determine the layer thickness δ from a balance between the turbulent transport of wall-normal fluctuations into the boundary,

$$|(\mathbf{u} \cdot \nabla) \mathbf{u}| \approx w_{rms}^2 / \delta, \quad (29)$$

and the viscous dissipation of such fluctuations,

$$\nu |\Delta \mathbf{u}| \approx \nu w_{rms} / \delta^2. \quad (30)$$

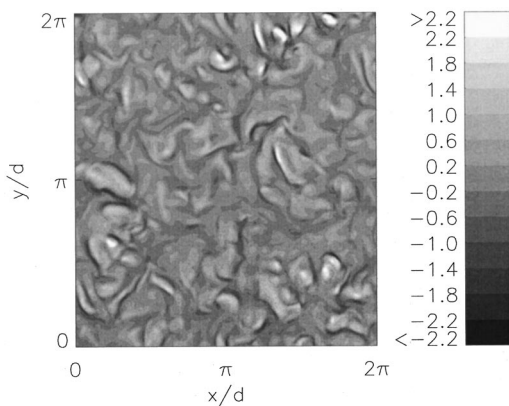


FIG. 7. Divergence $\hat{\nabla} \cdot \hat{\mathbf{u}}$ of the surface flow in units of the Kolmogorov time τ_η . Data are the same as for Fig. 6.

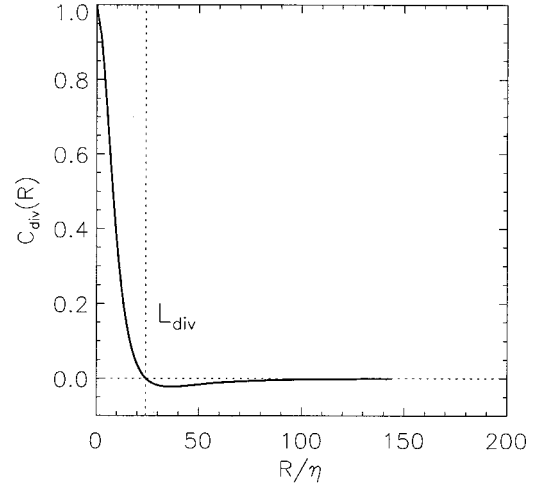


FIG. 8. Radially averaged correlation function of the divergence field for $Re_\lambda = 99$. The decorrelation length L_{div} is indicated by the vertical dotted line.

In both cases the size of the velocity field is estimated by the root mean square average of the wall-normal velocity fluctuations, w_{rms} . Equating the two expressions gives

$$\delta \approx \nu / w_{rms} \quad (31)$$

as an estimate of the thickness. This is compared with numerical data in Fig. 9 where the z profiles of the wall-normal fluctuations w_{rms} for two values of Taylor Reynolds number are shown. The boundary layer becomes smaller with increasing Re_λ , as expected. The absolute values for the thickness of the boundary layer can be read off from the data by linear extrapolations of the profile slopes at the surfaces. The intersections of these straight lines with the corresponding maximum values of w_{rms} were used to define the boundary

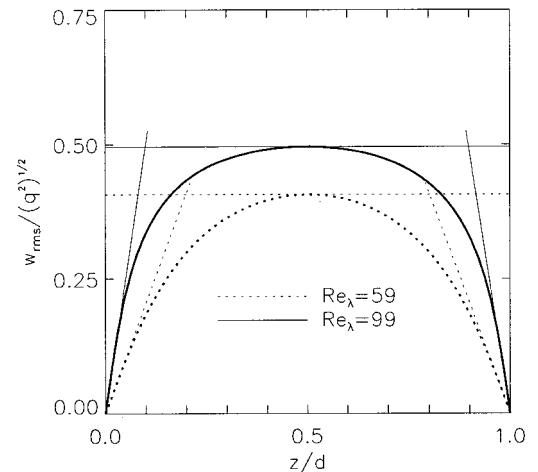


FIG. 9. Fluctuations of the normal velocity component as a function of the position between the surfaces. The fluctuations are normalized in units of the square root of the mean turbulent kinetic energy $q^2 = \langle u^2 \rangle_V + \langle v^2 \rangle_V + \langle w^2 \rangle_V$. A linear extrapolation from the surface up to the value in the middle gives a boundary layer thickness $\delta = 0.2$ for $Re_\lambda = 59$ and $\delta = 0.1$ for $Re_\lambda = 99$. This is about a factor of 10 larger than the values estimated from Eq. (31).

layer thickness (see Fig. 9). This gives values for δ that are about a factor of 10 larger than the dimensional estimate, but consistent with its scaling behavior. This estimate for the thickness of a surface layer agrees with the interval over which the scaling exponents in (Fig. 3) change from bulk to surface values.

IV. PASSIVE SCALAR TRANSPORT IN THE FREE-SLIP SURFACE

A. Time scales

Experimental and numerical studies show that the particles floating on the surface of a fluid cluster in regions with downwelling and avoid regions with upwelling motion [5,6]. The patterns that appear have huge density variations that are best described by fractal scaling exponents. As an approximation to the dynamics of particles we can study the advection of a scalar density on the surface: it differs from true particles in that it has no inertia (the importance of which can be reduced in experiments by sufficiently small and light particles; see, however, [25,26]) and that it can develop larger gradients.

Allowing for the compressibility of the flow field, the equations for the scalar density are thus

$$\partial_t \phi + \hat{\mathbf{V}} \cdot (\hat{\mathbf{u}} \phi) = D \hat{\Delta} \phi + f_\phi, \quad (32)$$

where D is the passive scalar diffusivity. The Prandtl number is $\text{Pr} = \nu/D$. The following discussion will be confined to the two-dimensional flow, so that all gradient, divergence, and Laplace operators act on the two coordinates x and y only; the carets will henceforth be omitted. Expanding the second term in the above expression then gives the evolution equation for the scalar,

$$\partial_t \phi = -(\mathbf{u} \cdot \nabla) \phi - (\nabla \cdot \mathbf{u}) \phi + D \Delta \phi + f_\phi. \quad (33)$$

The input f_ϕ in scalar density is needed in order to compensate the diffusive losses. Since the equation for the scalar is linear, the natural amplitude scale for ϕ is set by its root mean square value $\phi_{rms} = \langle \phi^2 \rangle^{1/2}$. After dividing by ϕ_{rms} all terms have dimensions of inverse time and the time scales involved can be used to characterize the different processes. Several of these processes also depend on the length scale l over which they are studied and so we introduce length scale resolved characteristic times. All terms can be made dimensionless using the inner scales of the turbulent velocity field in the surface, as discussed above Eq. (20). Different estimates of ϵ bring in factors of order 1 [see, e.g., relation (27) and the remarks below Eq. (20)]. Again, we use the energy dissipation rate that is given by Eq. (20) to compose η , v_η , and τ_η .

The advection term $(\mathbf{u} \cdot \nabla) \phi$ in Eq. (33) is characterized by the advective time scale

$$\tau_{adv}(l) = l/u(l) = \frac{\eta}{v_\eta} \left(\frac{l}{\eta} \right)^{2/3} = \tau_\eta \left(\frac{l}{\eta} \right)^{2/3} \quad (34)$$

where the scale resolved velocity $u(l) \approx v_\eta (l/\eta)^{1/3}$ in Kolmogorov theory. The next term in Eq. (33) contains the divergence of the 2D surface flow and acts like a source or sink for the scalar. Its time scale is denoted $\tau_{div}(l)$. The compressibility factor relates the divergence of the flow field to the root mean square velocity gradient [see Eq. (25)] which is connected with the energy dissipation rate ϵ and thus the Kolmogorov time τ_η . Numerical simulations and experiment [13] indicate $\tau_{div}(l) \approx \tau_\eta / C^{1/2}$, where C is the compressibility factor (26) with a value of about 1/2. The efficiency of diffusion clearly depends on l , so that the time scale $\tau_{diff}(l)$ for diffusive smearing is $\tau_{diff}(l) \approx l^2/D$. Finally, we have the forcing time $\tau_f = \phi_{rms}/f_\phi$, which again is independent of spatial resolution.

In any given range of length scales, the process with the shortest time scale can be expected to dominate. So starting from the smallest scales we expect for an incompressible fluid first a diffusion dominated regime, then an advection dominated one, and finally the input dominated regime. A Batchelor regime for the scalar is found if the diffusive regime extends beyond the Komogorov length, i.e., $\text{Pr} \gg 1$. In an incompressible flow, $C=0$ and τ_{div} is infinite, so that there is no influence from the divergence. In the surface flows studied here, the estimate for C indicates that τ_{div} is very short, of the order of the Kolmogorov time. This implies that the advective regime is suppressed and that the statistics of the divergence dominates. This, finally, explains why the properties of the hydrodynamic flow do not seem to matter too much in the analysis of the particle distribution on free surfaces and why Ott *et al.* could explain the experiments using random maps [3–6].

B. Application of geometric scaling theory

In order to connect the scaling of the velocity field to the scaling properties of the scalar, we use geometric measure theory [27] and the scaling ideas developed by Constantin and co-workers [28–30]. A further extension of their work allowed for a scale resolved and Prandtl number dependent analysis [31,9]. The basic idea of the approach is to relate the fractal dimension $\delta_g^{(2)}$ of the passive scalar concentration, i.e., the scaling exponent (with respect to R) of the Hausdorff volume H of the passive scalar graph $G(B_R^{(2)}) = \{(\mathbf{x}, \phi) | \mathbf{x} \in B_R^{(2)}, \phi = \phi(\mathbf{x})\}$ taken over a two-dimensional ball $B_R^{(2)}$ of radius R , to scaling properties of the underlying turbulent flow that mixes the scalar. The following discussion will focus on the additional terms relevant to the current problem; more details can be found in the above mentioned references [28–31] and our previous work [9].

The basic quantity to be calculated within geometric measure theory is the relative Hausdorff volume of a surface of the normalized scalar density $\tilde{\phi} = \phi/\phi_{rms}$, as given by

$$\frac{H(G(B_R^{(2)}))}{V(B_R^{(2)})} \sim R^{\delta_g^{(2)} - 2} \leq \sqrt{1 + \frac{1}{\pi} \int_{B_R^{(2)}} |\nabla \tilde{\phi}|^2 d^2 \mathbf{x}}, \quad (35)$$

where $V(B_R^{(2)}) = \pi R^2$ is the volume of a two-dimensional ball with radius R . The scaling exponent of the first order

scalar structure function and fractal dimensions can be related by inequalities, which for the analysis are assumed to be sharp [29]. Using the relation $\phi\Delta\phi = \Delta\phi^2/2 - |\nabla\phi|^2$ and the equation of motion (33), the gradient under the integral can be replaced by

$$|\nabla\tilde{\phi}|^2 = -\frac{1}{2D}(\mathbf{u}\cdot\nabla)\tilde{\phi}^2 - \frac{1}{D}\tilde{\phi}^2(\nabla\cdot\mathbf{u}) + \frac{1}{2}\Delta\tilde{\phi}^2 + \frac{f_\phi\tilde{\phi}}{D\phi_{rms}}. \quad (36)$$

With

$$(\mathbf{u}\cdot\nabla)\tilde{\phi}^2 = \nabla\cdot(\mathbf{u}\tilde{\phi}^2) - \tilde{\phi}^2(\nabla\cdot\mathbf{u}) \quad (37)$$

the first term on the right hand side can be expressed as a sum of two divergences. When substituted under the integral in Eq. (35) the Hausdorff volume becomes

$$\frac{H(G(B_R^{(2)}))}{V(B_R^{(2)})} \leq \sqrt{1 + \frac{1}{\pi} \int_{B_R^{(2)}} \left\{ \frac{1}{2D} [-\nabla\cdot(\mathbf{u}\tilde{\phi}^2) - \tilde{\phi}^2(\nabla\cdot\mathbf{u}) + D\Delta\tilde{\phi}^2] + \frac{f_\phi\tilde{\phi}}{D\phi_{rms}} \right\} d^2\mathbf{x}}. \quad (38)$$

The four integrals are denoted I_1 through I_4 and analyzed separately. The analysis of the three integrals I_1 , I_3 , and I_4 proceeds as in the previous applications to two-dimensional scalar advection [9]. In particular, application of Gauss's theorem and the Cauchy-Schwartz inequality connects the first integral to the longitudinal structure function of the surface velocity field $S_2^L(R)$,

$$I_1 \leq \frac{\sqrt{F_\phi}}{D} R \sqrt{S_2^L(R)}. \quad (39)$$

F_ϕ is the flatness of the passive scalar,

$$F_\phi = \langle \phi^4 \rangle / \langle \phi^2 \rangle^2 = \langle \tilde{\phi}^4 \rangle. \quad (40)$$

If the correlations of ϕ decay rapidly this is essentially the volume average $\langle \phi^4 \rangle_V / \langle \phi^2 \rangle_V^2$. For a Gaussian velocity field, $F_\phi = 3$. Experiments and numerical simulations indicate strong ramp and cliff structures in the scalar field and thus some deviation from the Gaussian distribution [32–35], implying a scale dependence of F_ϕ . However, we here restrict ourselves to first and second order correlations where intermittency corrections to the classical Kolmogorov-Obukhov-Corrsin scaling are expected to be small and work with a constant F_ϕ .

Exploiting the statistical stationarity of the passive scalar dynamics the fourth term, which contains the driving of the passive scalar, can be expressed as

$$\begin{aligned} I_4 &= \frac{1}{\pi} \int_{B_R^{(2)}} \frac{f_\phi\tilde{\phi}}{D\phi_{rms}} d^2\mathbf{x} \\ &= \frac{R^2}{D\phi_{rms}^2} \frac{1}{\pi R^2} \int_{B_R^{(2)}} f_\phi\phi d^2\mathbf{x} \\ &= \text{Pr} \frac{\tau_\eta \tilde{R}^2}{\tau_f}, \end{aligned} \quad (41)$$

where $\tilde{R} = R/\eta$ is the radius of the disk in units of the Kolmogorov length. Using Gauss's theorem and Green's formula it can be shown [9] that the third term is subdominant compared to the fourth,

$$I_3 \leq 2\sqrt{I_4} \propto \tilde{R}, \quad (42)$$

and hence can be omitted in the following.

Finally, we come to the term I_2 , which contains the divergence of the velocity field. Application of the Cauchy-Schwartz inequality gives

$$\begin{aligned} I_2 &= -\frac{1}{2\pi D} \int_{B_R^{(2)}} \tilde{\phi}^2(\nabla\cdot\mathbf{u}) d^2\mathbf{x} \\ &\leq \frac{R^2}{2D} \sqrt{\int_{B_R^{(2)}} \frac{\tilde{\phi}^4}{V(B_R^{(2)})} d^2\mathbf{x}} \sqrt{\int_{B_R^{(2)}} \frac{(\nabla\cdot\mathbf{u})^2}{V(B_R^{(2)})} d^2\mathbf{x}} \\ &= \frac{\sqrt{F_\phi} R^2}{2D} \langle (\nabla\cdot\mathbf{u})^2 \rangle^{1/2} \\ &= \frac{\sqrt{F_\phi} \text{Pr} \tilde{R}^2}{2} \langle (\tilde{\nabla}\cdot\mathbf{u})^2 \rangle^{1/2}, \end{aligned} \quad (43)$$

where the root mean square of the divergence is measured in units of the Kolmogorov time τ_η . The derivatives in the divergence term can be estimated from above using $\langle (\nabla\cdot\mathbf{u})^2 \rangle \leq \langle |\nabla\mathbf{u}|^2 \rangle$ [see Eq. (25)]. In the following calculation this bound is not needed and the divergence fluctuations in Eq. (43) can be taken directly from the numerical simulations.

Combining Eqs. (38), (39), and (41) we arrive at an inequality for the fractal dimension $\delta_g^{(2)}$ of the passive scalar graph and thus via $\delta_g^{(1)} = \delta_g^{(2)} - 1$ [29] at a fractal dimension for the constant level sets $\phi_0 = \phi(\mathbf{x})$,

$$\delta_g^{(1)} - 1 \leq \frac{d}{d \ln \tilde{R}} \ln h(\tilde{R}), \quad (44)$$

with

$$h(\tilde{R}) = \sqrt{1 + \sqrt{F_\phi} \text{Pr} \tilde{R} \sqrt{\tilde{S}_2^L} + \frac{\sqrt{F_\phi} \text{Pr} \tilde{R}^2}{2} \langle (\tilde{\nabla} \cdot \mathbf{u})^2 \rangle^{1/2} + \text{Pr} \frac{\tau_\eta}{\tau_f} \tilde{R}^2}. \quad (45)$$

$\tilde{S}_2^L = S_2^L / v_\eta^2$ is the longitudinal second order structure function in units of the Kolmogorov velocity. Obviously, if the last two terms under the integral dominate, then $h(\tilde{R}) \approx \tilde{R}$ and $\delta_g^{(1)} = 2$, implying a surface filling distribution of the scalar. For sufficiently large scales \tilde{R} or large Prandtl numbers this is always the case. On the other hand, if the second term with the velocity structure function dominates, say $\tilde{S}_2^L \approx \tilde{R}^\gamma$, then $\delta_g^{(1)} = 3/2 + \gamma/4$. Thus for the usual Kolmogorov scaling $\tilde{S}_2^L \sim \tilde{R}^{2/3}$ and $\delta_g^{(1)} = 5/3$.

The Prandtl number dependence of the fractal dimension can be studied using as input the velocity correlation functions from our numerical simulations. Both Pr and the prefactor τ_η/τ_f , a measure of the strength of the scalar driving, are free parameters in Eq. (45). The results for two different values of τ_η/τ_f are shown in Fig. 10. For many values of Pr a fractal dimension $\delta_g^{(1)} < 2$ is observed. If the term τ_η/τ_f becomes large, either because of a small τ_f (strong driving) or a large τ_η (weak transport to smaller scales), the fractal dimension approaches that of a space filling fractal, $\delta_g^{(1)} \approx 2$.

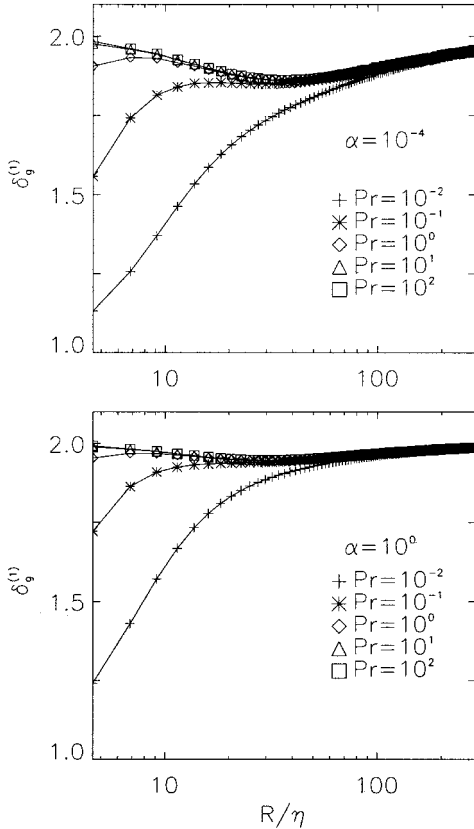


FIG. 10. Fractal dimension $\delta_g^{(1)}$ for passively advected scalars for different values of the parameter $\alpha = \tau_\eta/\tau_f$ and the Prandtl number Pr. The underlying turbulent velocity field is the surface flow for $\text{Re}_\lambda = 99$ as shown in Fig. 2 and $F_\phi = 3$.

In the experiments of Sommerer [6] a fractal dimension $\delta_g^{(1)}$ between 1.28 and 1.43 (denoted D_2) was found. We find these values only in the transitional region, before the inertial range is developed. The observations are consistent with Eq. (45) since it provides only an upper bound and the observed values are indeed smaller. Further comparisons between experiment and theory, using, e.g., measured velocity correlation functions in Eq. (45), would be more than welcome. Some experiments are in preparation [13].

V. SUMMARY

The surface flows studied here are intermediate between two- and three-dimensional flows. They are confined to a surface, but their statistical properties are strongly influenced, even dominated, by the 3D volume turbulence. The flow field in the surface can exchange energy and vorticity with the bulk, so that neither energy nor enstrophy are conserved quantities in the Eulerian, undriven limit. Moreover, in addition to large scale forces that maintain the 3D flow the surface flow is driven by small scale perturbations that come from transverse pressure variations and local gradients in normal velocity. As a result the scaling properties of the flow are essentially those of 3D turbulence, with an energy cascade in the inertial regime. The scaling exponents of the velocity structure function are slightly larger than those of bulk 3D turbulent flows, indicating larger intermittency effects. We also observed a 2/3 difference in the amplitude of the structure functions between surface and bulk in the inertial regime. Several of the observed characteristics of the surface flow are in agreement with the measurements of Goldberg *et al.* [13].

We have also discussed the scaling properties of a scalar advected by the surface flow and have identified different scaling regimes. It seems that very often the dynamics induced by the divergence of the flow field is the fastest process, and that the advective properties of the flow are subdominant. This might explain why random mappings could successfully be applied to the modeling of the particle distributions [3–6], but a more detailed comparison between theory and experiment is clearly needed.

An important characteristic quantity of the surface flows is the compressibility factor \mathcal{C} . The numerical simulations and the experiment [13] using a vertically oscillating grid both indicate $\mathcal{C} \approx 1/2$. With a stable stratification of the fluid below the surface that reduces vertical fluctuations it might be possible to achieve smaller values of \mathcal{C} . This should open up the possibility of studying the effects of compressibility over a larger range of \mathcal{C} , in connection both with the intermittency contributions to the scaling exponents and with the scalar dynamics in surface flows.

ACKNOWLEDGMENTS

B.E. would like to thank Walter Goldburg for raising the problem of surface flows and Luca Biferale for a discussion of time scales. We thank Rainer Friedrich and Detlef Lohse for suggesting supersonic compressible turbulence to us. Both of us would like to thank the Institute for Theoretical

Physics at Santa Barbara for hospitality. This work was supported in part by the National Science Foundation under Grant No. PHY94-07194, and the EU within the CARTUM project and the “Nonideal turbulence” Research Training Network HPRN-CT-2000-00162. The numerical simulations were done on a Cray T-90 at the John von Neumann–Institut für Computing at the Forschungszentrum Jülich and we are grateful for their support.

-
- [1] H. Stommel, *J. Mar. Res.* **8**, 199 (1949).
 [2] R. E. Davis, *Annu. Rev. Fluid Mech.* **23**, 43 (1991).
 [3] L. Yu, E. Ott, and Q. Chen, *Phys. Rev. Lett.* **65**, 2935 (1990).
 [4] T. Antonsen, A. Namenson, E. Ott, and J. C. Sommerer, *Phys. Rev. Lett.* **75**, 3438 (1995).
 [5] A. Namenson, T. Antonsen, and E. Ott, *Phys. Fluids* **8**, 2426 (1996).
 [6] J. C. Sommerer, *Phys. Fluids* **8**, 2441 (1996).
 [7] V. I. Klyatskin and A. I. Saichev, *Zh. Éksp. Teor. Fiz.* **111**, 1297 (1997) [*JETP* **84**, 716 (1997)].
 [8] A. I. Saichev and I. S. Zhukova, Vol. 511 of *Lecture Notes in Physics* (Springer, Berlin 1998), p. 353.
 [9] B. Eckhardt and J. Schumacher, *Phys. Rev. E* **60**, 4185 (1999).
 [10] B. K. Martin, X. L. Wu, W. I. Goldburg, and M. A. Rutgers, *Phys. Rev. Lett.* **80**, 3964 (1998).
 [11] M. Rivera, P. Vorobieff, and R. E. Ecke, *Phys. Rev. Lett.* **81**, 1417 (1998).
 [12] M. A. Rutgers, *Phys. Rev. Lett.* **81**, 2244 (1998).
 [13] W. I. Goldburg, J. R. Cressman, Z. Vörös, B. Eckhardt, and J. Schumacher, *Phys. Rev. E* **63**, 065303 (2000).
 [14] U. Frisch, *Turbulence, The Legacy of A. N. Kolmogorov* (Cambridge University Press, Cambridge, 1995).
 [15] N. Seehafer, E. Zienicke, and F. Feudel, *Phys. Rev. E* **54**, 2863 (1996).
 [16] J. Schumacher and B. Eckhardt, *Europhys. Lett.* **52**, 627 (2000).
 [17] R. Benzi, S. Ciliberto, R. Tripiccion, C. Baudet, F. Massaioli, and S. Succi, *Phys. Rev. E* **48**, R29 (1993).
 [18] K. Gawędzki and M. Vergassola, *Physica D* **138**, 63 (2000).
 [19] A. Celani, A. Lanotte, and A. Mazzino, *Phys. Rev. E* **60**, R1138 (1999).
 [20] D. H. Porter, P. R. Woodward, and A. Pouquet, *Phys. Fluids* **10**, 237 (1998).
 [21] J. Pety and É. Falgarone, *Astron. Astrophys.* **356**, 279 (2000).
 [22] V. E. Zakharov, V. S. L’vov, and G. Falkovich, *Kolmogorov Spectra of Turbulence I: Wave Turbulence* (Springer-Verlag, Berlin, 1992).
 [23] S. Grossmann and P. Mertens, *Z. Phys. B: Condens. Matter* **88**, 105 (1992).
 [24] J. Schumacher and B. Eckhardt, *Phys. Plasmas* **6**, 3477 (1999).
 [25] A. Babiano, J. H. E. Cartwright, O. Piro, and A. Provenzale, *Phys. Rev. Lett.* **84**, 5764 (2000).
 [26] E. Balkovsky, G. Falkovich, and A. Fouxon, *Phys. Rev. Lett.* **86**, 2790 (2001).
 [27] H. Federer, *Geometric Measure Theory* (Springer, Berlin, 1969).
 [28] P. Constantin, I. Procaccia, and K. R. Sreenivasan, *Phys. Rev. Lett.* **67**, 1739 (1991).
 [29] P. Constantin and I. Procaccia, *Phys. Rev. E* **47**, 3307 (1993).
 [30] I. Procaccia and P. Constantin, *Europhys. Lett.* **22**, 689 (1993).
 [31] S. Grossman and D. Lohse, *Europhys. Lett.* **27**, 347 (1994).
 [32] K. R. Sreenivasan, R. A. Antonia, and D. Britz, *J. Fluid Mech.* **94**, 745 (1979).
 [33] M. Holzer and E. D. Siggia, *Phys. Fluids* **6**, 1820 (1994).
 [34] L. Mydlarski and Z. Warhaft, *J. Fluid Mech.* **358**, 135 (1998).
 [35] A. Celani, A. Lanotte, A. Mazzino, and M. Vergassola, *Phys. Rev. Lett.* **84**, 2385 (2000).